Version of Record: https://www.sciencedirect.com/science/article/pii/S0013468623012549
Manuscript_d5322aeec030ede41c909a2f61418fc5

Hydrodynamic Voltammetry of $Fe^{2+/3+}$ in Aqueous Deep Eutectic Solvents Towards Redox Flow Batteries

Desiree Mae Prado [a], *Xiaochen Shen* [b], *Robert Savinell* [b, *], *Clemens Burda* [a, *]

[a] Department of Chemistry, Case Western Reserve University, Cleveland, OH 44106, USA

[b] Department of Chemical and Biomolecular Engineering, Case Western Reserve University, Cleveland, OH 44106, USA

E-mail Address of Authors:

Desiree Mae Prado – dxp421@case.edu

Xiaochen Shen – xxs322@case.edu

Corresponding Authors

[a, *] Clemens Burda

Department of Chemistry, Case Western Reserve University, Cleveland, OH 44106, USA;

E-mail: burda@case.edu ; Tel. No.: +1 216 368 5918

[b, *] Robert Savinell

Department of Chemical and Biomolecular Engineering, Case Western Reserve University, Cleveland, OH 44106, USA; E-mail: rfs2@case.edu ; Tel. No.: +1 216 368 2728

© 2023 published by Elsevier. This manuscript is made available under the Elsevier user license
https://www.elsevier.com/open-access/userlicense/1.0/

Abstract

Deep eutectic solvents (DESs) have recently attracted much attention as potential green electrolyte solvents for redox flow batteries. DESs are considered not only as environmentally sustainable but also economically attractive electrolytes because they can be resourced from biological feedstock (alcohols, urea, choline) and are earth-abundant and of low toxicity. Despite these advantages, DESs still have limitations in important aspects such as reactant and ion transport, which is inhibited due to hydrogen-bonding-induced viscosity. Thus, improving the transport properties of redox species in DESs is essential. In addition, we explore the quantitative addition of water to ethaline (a 1:2 choline chloride: ethylene glycol mixture) in order to understand its influence on the kinetics and mass transport properties of DESs. In this work, we show that DESs can be made more fluid and less dense, while avoiding most of the electrochemical instabilities of water. Herein, we investigate the effects of gradually increasing amounts of water to the redox system of $Fe^{2+/3+}$ in ethaline. Our study shows that systematic addition of water leads to a three-fold increase in ionic conductivity and decrease in viscosity that enhances the mass transport and kinetics of DES-based electrolytes while still maintaining an electrochemical window of approximately 1.90 V. The use of environmentally benign electrolyte components together with the observed increase in conductivity will result in a more efficient redox flow battery (RFB) that operates at higher power density without relying on harmful solvents and fossil fuel-based processes.

***Keywords*:** deep eutectic solvent; redox flow battery; hydrodynamic voltammetry; redox couple; renewable energy

1. Introduction

The increasing global energy demand and related carbon dioxide emissions have spurred interest in the transition from traditional fossil fuels to renewable energies, which are most common in the form of solar and wind energies.[1,2] Although solar and wind energies have the advantage of being low-carbon and long-term energy sources; they suffer from being inherently intermittent and less flexible.[3,4] To address these challenges, various energy storage systems can be integrated with a renewable energy source.[5] For example, pump hydroelectric storage dominates the existing energy storage systems. However, it is limited by the very large land footprint as it requires to build two large reservoirs at different elevations. Considering other energy storage systems, redox flow batteries (RFBs) store more energy while delivering high power loads compared to conventional batteries. [6] In comparison with the lithium-ion battery that has attracted commercial attention, RFBs are potentially of lower cost, longer lifetime, safer, and easier to recycle.[5,7]

In a typical RFB, the electrolyte containing the active species is stored in two external tanks as seen in Scheme 1. One tank is for the storage of the negative electrolyte, and the other tank is for the storage of the positive electrolyte.[8] During operation, the electrolytes are pumped into the flow battery stack, which has positive and negative electrode compartments. These two fluids are separated by an ion-exchange membrane which allows the charge carriers to move between two electrolytes to balance the charge during operation while restricting the mixing of the two electrolytes. Energy can then either be stored or extracted from the RFB by changing the oxidation state of electrolyte fluids.[9] Hence, the electrolyte is an essential part of the RFB. It closes the electronic and ionic circuit between the anode and cathode. In a liquid flowing electrolyte systems like in an RFB, low-viscosity electrolyte is essential to yield a faster ionic transport and enhanced ionic conductivity.

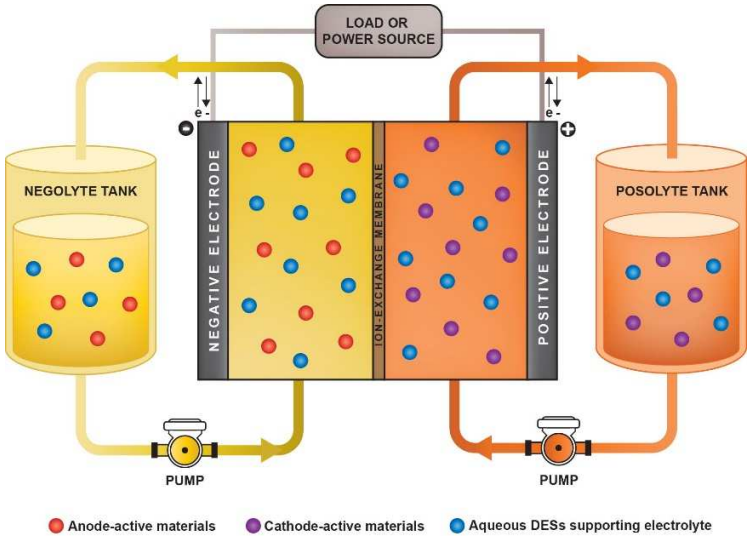

Scheme 1. Schematic diagram of a redox flow battery. The active materials and the supporting electrolytes are stored in the external electrolyte tanks. In RFBs, increased electrolyte fluidity is desired to improve the ion mobility and conductivity of electroactive species.

Deep eutectic solvents (DESs) gained attention as potential suitable green electrolytes for RFBs.[10–12] DESs are an emerging class of mixtures of hydrogen-bond donor molecules and hydrogen-bond acceptor molecules that are characterized by a significant depression of its melting point compared to that of its individual constituents.[13] They share properties with ionic liquids (ILs), such as low volatility, high thermal and chemical stability, and tunable polarity.[14,15] However, DESs possess additional advantages, which includes low cost, non-toxicity, and ease of preparation.[16,17] On the other hand, DESs being non-aqueous electrolytes, often have limited solubility for electroactive species due to the low solvent dielectric constant. This can be improved by using electroactive salts such as iron chlorides as the hydrogen-bond acceptor,[18] or even functionalizing the constituent molecules of the DES with electroactive groups.[19–21] The dynamics and electrokinetics of various electroactive salts in traditional liquid electrolytes, such as aqueous and organic electrolytes, have already been established.[22–25] However, these electrolytes are limited by their narrow potential window, high volatility, and high toxicity, which

makes them not ideal for RFB applications.[26,27] Investigating the use of completely replenishable and sustainable electrolyte components is necessary for future energy storage and conversion.

DESs can be made by sustainable processes, [28] but suffer from physical limitations of high viscosity, and consequently, low ionic conductivity, and diffusivity of redox active species.[29] To address these constraints, incorporation of minor amounts of water can be exploited since it disrupts the strong hydrogen bond network between the DES components,[30] which can reduce the viscosity and enhance transport properties. This work aims to study the analytical addition of water as a minority solvent component to the DESs and its effects on transport kinetics. We examine the effect of water addition on DES by electrochemical measurements including electrochemical impedance spectroscopy, cyclic voltammetry, and linear sweep voltammetry of the well-established redox couple $Fe^{2+/3+}$ for reference. A systematic addition of water lowers viscosity, increases ionic conductivity and diffusion coefficients, reduces density, while preserving the electrochemical stability window. This study reveals that the addition of analytical amounts of water to eutectic solvent mixtures provides a technologically viable basis for improving flow battery performance.

2. Experimental methods

2.1. Chemical reagents

The anhydrous ethylene glycol (EG, ≥99% purity), choline chloride (ChCl, ≥99% purity), and anhydrous iron (II) chloride ($FeCl_2$, 98% purity) were purchased from Sigma Aldrich. The anhydrous iron (III) chloride ($FeCl_3$, 98% purity) was purchased from Fischer Scientific. The

water used in this experiment was purified using a Millipore Milli-Q system to a resistivity of 18.2 MΩ cm.

2.2. Sample preparation

The ethylene glycol was dried using activated molecular sieve for 48 h while the choline chloride was dried under vacuum for 48h at 373 K to remove adsorbed water. The dried choline chloride and ethylene glycol were mixed in a 1:2 molar ratio inside an argon-filled glovebox to produce a DES which is commonly named ethaline. The DES mixture was then placed in a sonicator for 30 min at 303 K to generate a clear ethaline solution which subsequently was cooled to room temperature. After that, $FeCl_2$ and $FeCl_3$ were dissolved in the previously prepared ethaline to a concentration of 50 mM $FeCl_2$ and 50 mM $FeCl_3$. To completely dissolve the iron salts, the mixture was heated to 303 K. Then predetermined amounts of water were added to the mixture to make 5, 10, and 25 wt.% added water samples. The $FeCl_2$ and $FeCl_3$ in aqueous-containing ethaline solution was then transferred and sealed into a 5-necked double-walled electrochemical cell. To minimize water adsorption from the atmosphere, the solution was saturated with high-purity nitrogen (N_2) gas throughout the measurements.

2.3. Water content determination

Karl Fischer titration (Metrohm Coulometer 899) was performed to provide a baseline for the water content in ethaline as base solvent without any additional water. That baseline water content was found to be below 1500 ppm.

2.4. Viscosity and density measurements.

A Rheosense microviscometer was used to measure the viscosity of the samples using a microfluidic chip calibrated for the range 1-100 cP. To measure the temperature-dependent viscosity of the samples, a Rheosense temperature controller was utilized. Density

measurements were taken using an Anton Paar density meter (DMA 5000 M) at temperatures in the rage of 298– 323 K in 5 K increments.

2.5. Conductivity measurements

Electrochemical impedance spectroscopy (EIS) was utilized to determine the conductivity of the samples. A cell with two platinum electrodes was filled with sample solutions. The impedance measurements were performed at 100 – 10,000 Hz to obtain a Nyquist plot. The solution resistances (R_s) of the samples were then determined by estimating where the high frequency data intercepts the real resistance axis. Using the measured resistance, the conductivity of samples was calculated using the eq. (1).

$$\sigma(mS \cdot cm^{-1}) = \frac{k\,(\mathrm{cm}^{-1})}{\rho\,(\mathrm{ohm})} \times 1000 \quad (1)$$

where σ is the conductivity, k the cell constant, and ρ is the solution resistance. The cell constant of the platinized cell was 1.0 cm^{-1}. To measure the conductivity of the samples at a controlled temperature, the cell was submerged in mineral oil heated on a digital hot plate with temperature probe.

The molar conductivity of the samples was calculated by plugging the measured conductivity values to eq. (2).

$$\Lambda\,(S \cdot cm^2 \cdot mol^{-1}) = \frac{\sigma\,(S \cdot cm^{-1})}{c\,(mol \cdot cm^{-3})} \quad (2)$$

where Λ is the molar conductivity, σ is the measured conductivity, and c is the molar concentration of the samples.

The viscosity, density, and conductivity data of the samples in the temperature range from 298 K to 323 K in 5 K increments are reported in Table S1.

2.6.Cyclic voltammetry (CV) and linear sweep voltammetry (LSV)

Cyclic voltammetry was performed at 100 mV s^{-1}, sweeping to positive potentials first from 0 V vs. the reference electrode. Electrolyte samples of 100 mL were placed in a multiport glass electrochemical cell with a 5 mm platinum (Pt) disc as the working electrode, a graphite rod as the counter electrode, and Pt/Fe^{2+}/Fe^{3+} (Pt RE) as the reference electrode. The Pt RE is constructed by introducing a platinized Pt wire into a Luggin capillary filled with a 50 mM $FeCl_2$/$FeCl_3$ ethaline electrolyte. The Luggin capillary is designed to have an opening near the working electrode, which allows the test solution to come in contact with the electrolyte. Electrochemical tests were controlled with a Biologic SP-240 potentiostat.

Utilizing the data obtained from the CV curves, the electrochemical stability window is determined employing eq. (3).

$$E_w = E_{ox} - E_{red} \tag{3}$$

where E_w is the electrochemical stability window, E_{ox} is the anodic oxidation potential limit, and E_{red} is the cathodic reduction potential limit.

For the linear sweep voltammetry, the same set-up was used with the sweeping rate set at 10 mV s^{-1}. The rotating disk electrode was spun at 900, 1200, 1600, 2000, 2200, and 2500 rpm using a Pine Instruments MSR rotator. All the electrochemical experiments were conducted in the temperature range of 298 – 323 K in 5 K increments using circulating water bath to stabilize each temperature.

2.7. Nuclear magnetic resonance (NMR) spectroscopy

The samples for NMR measurements were prepared by dissolving dry or water-containing $Fe^{2+/3+}$ -ethaline solutions in deuterium oxide (D_2O) at a ratio of 1:1 after they were exposed to a potential bias of 350 mV beyond anodic and cathodic limiting voltage at which decomposition occurred in ethaline-water mixtures. A 500 MHz Bruker-Bio Spin Avance III HD spectrometer

fitted with an incredibly high sensitivity Multinuclear Broadband CryoProbe was used to obtain NMR spectra at 298 K. The measurements of ^{1}H-NMR, and ^{13}C-NMR were taken using the operational magnetic field of 11.7 T.

2.8. Atomic absorption spectroscopy (AAS)

The solubility of $FeCl_2$/$FeCl_3$ in the samples was measured by saturating the samples with the iron chloride salts until no more salt dissolved after sonication at 298 K for 2 hours. An Agilent 240 FS flame atomic absorption spectrometer was then utilized to measure the concentration of Fe ions dissolved in the saturated samples. An Fe hollow cathode lamp operating at 372.0 nm was used as the radiation source. A standard Fe calibration curve was constructed to determine the levels of Fe in the water-containing ethaline samples. This was achieved by utilizing the Agilent's Sample Introduction Pump Systems (SIPS) by performing in-line dilution of 1000 ppm in 2% HNO_3 stock solution (TraceCERT®, Sigma Aldrich), and subjecting the 0, 5, 10, 15, and 25 ppm Fe standard solutions to AAS analysis using a premixed burner air-acetylene flame. The same experimental conditions were then used to analyze the Fe content of the ethaline-water mixtures, with the constructed calibration curve used to determine the concentrations of Fe in each sample.

3. Results and Discussion

3.1. Viscosity, density, ionic conductivity, and Walden plot

To determine the influence of water addition to the transport and kinetics properties of Fe^{2+} and Fe^{3+} ions in ethaline (a 1:2 mixture of choline chloride and ethylene glycol), 50 mM $FeCl_2$/$FeCl_3$ was added to all solutions.

In Figure 1a, with gradually increasing amounts of water, the temperature-dependent viscosity of $Fe^{2+/3+}$-ethaline samples decreases. The viscosity of dry $Fe^{2+/3+}$-ethaline at 298 K is 49.85 cP, which is comparable to the previously reported value. [31] Upon addition of 25 wt. % water, the temperature-dependent viscosity of $Fe^{2+/3+}$-ethaline decreased by about 80%. Such a drastic decrease in viscosity can be attributed to the weakening of intermolecular hydrogen bond interactions between the DESs components due to the interference of water.[30] As seen in Figure 1b, as water is added to $Fe^{2+/3+}$-ethaline, the temperature-dependent density of the mixture decreased linearly in the investigated range. Similarly, the fluidity and the ion mobility are expected to increase with water addition, by which the temperature-dependent conductivity is improved as shown in Figure 1c. More than three-fold increase in the temperature-dependent conductivity of Fe^{2+}/Fe^{3+} - ethaline is observed upon addition of 25 wt. % water.

In Figure 1d, the Walden plot of temperature-dependent molar conductivity versus fluidity, which is the inverse of viscosity, was plotted to assess the ionicity of the deep eutectic solvent systems. It should be noted that the Walden plot does not specifically take into account the variation in ion sizes. The ideal 0.01 $mol \cdot L^{-1}$ aqueous KCl line is represented by the dashed line across the origin, which is provided for reference. This reference line represents the case where the ions are completely dissociated and equally mobile.[32] The addition of increasing amounts of water causes a smaller deviation from the reference line, which means that the ionicity of DES increases as more water is added to the mixture. This increase in ionicity supports the significant enhancement in conductivity seen in Figure 1c.

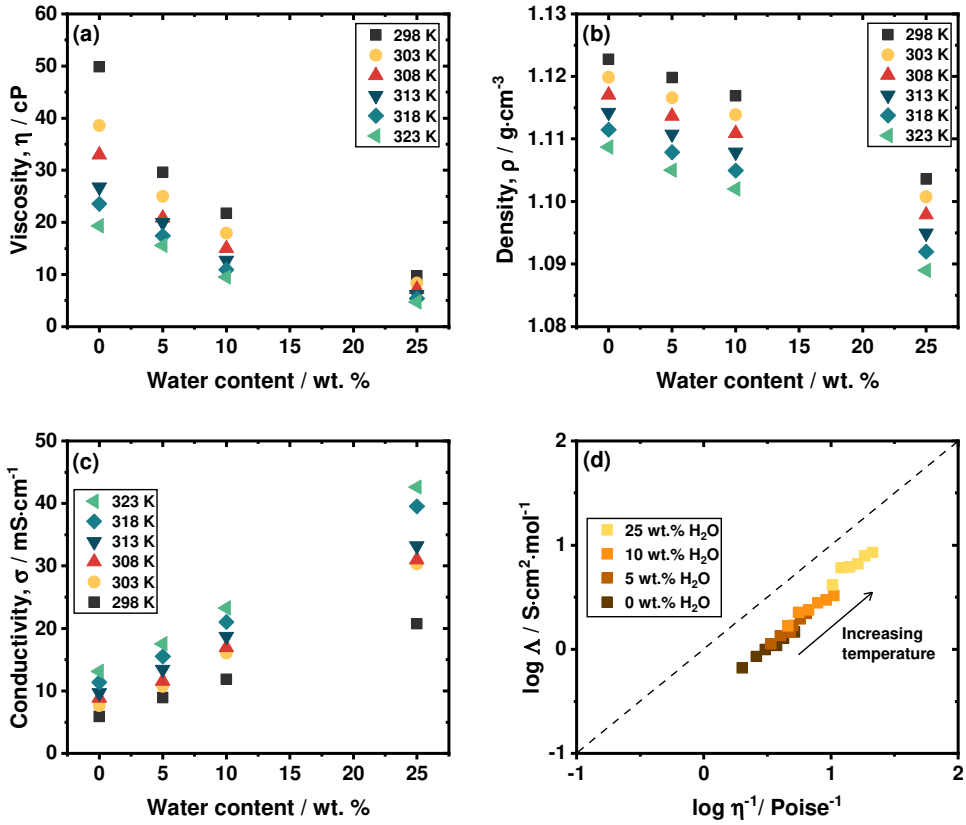

Figure 1. Effect of water addition and temperature increase on the (a) viscosity (η), (b) density (ρ), and (c) ionic conductivity (σ) of $Fe^{2+/3+}$-ethaline solutions. The (d) Walden plot of temperature-dependent molar conductivities (Λ) and fluidity (inverse of viscosity, η^{-1}) for water-containing $Fe^{2+/3+}$-ethaline. The dashed line through the origin with a slope of 1 represents the ideal line for 0.01 mol·L^{-1} aqueous KCl.

Consequently, an increase in the temperature induces a decrease in viscosity and density, and an increase in conductivity and ionicity as observed in Figure 1a-d. The decrease in viscosity and enhancement in conductivity with increasing temperature has been also observed in previous study.[33] When the temperature was increased from 298 K to 323 K, the conductivity of ethaline increased from 5.91 mS·cm^{-1} to 13.15 mS·cm^{-1}.

To determine the amount of water that would result in an equivalent increase in conductivity as the temperature range of 298 to 323 K, a linear fit was constructed using the data obtained from the relationship between conductivity and water content, as shown in Figure S1. By employing the

linear fit equation, the water content at which the conductivity reached 13.15 $mS \cdot cm^{-1}$ was determined. This conductivity value is comparable to that obtained by raising the temperature from 298 K to 323 K. The calculated result indicated that achieving a conductivity of 13.15 $mS \cdot cm^{-1}$ would require a water content of 12.15 wt. %. Previous studies have extensively reported on the properties of ethaline-water mixtures in the absence of iron chloride salts, specifically focusing on their viscosity, density, and conductivity. [30,34] Our study investigates the effect of introducing dissolved iron chloride salts into similar compositions of wet ethaline. To assess the impact of these salts on the viscosity, density, and conductivity, a comparative analysis was conducted between the ethaline-water mixture with and without the addition of iron chloride salts, as depicted in Figure S2.

The analysis reveals noteworthy findings: Firstly, the viscosity of the ethaline-water mixture remains unchanged upon the addition of iron chloride salts. Secondly, the density of the mixture shows an increase with the inclusion of iron chloride salts. Lastly, the conductivity of the mixture exhibits a decrease when the salts are introduced, with this trend persisting across the temperature range of 298 to 323 K.

Furthermore, when water is introduced into the mixture, similar trends in viscosity, density, and conductivity are observed, except for the viscosity at a water content of 10 wt. %, where a slight decrease occurs upon the addition of iron chloride salts.

3.2. Electrochemical stability window and NMR spectroscopy

Electrochemical stability window is defined as the voltage range at which the $Fe^{2+/3+}$-ethaline mixtures, containing 0, 5, 10, or 25 wt.% water, show no detectable signs of chemical

decomposition. This electrochemical stability range can be determined using cyclic voltammetry (CV).

The electrochemical stability window (E_w) can be extracted from the CV curves using eq. (3), which calculates it as the difference between the anodic oxidation potential limit, E_{ox}, and cathodic reduction potential limit, E_{red}. The E_{ox} and the E_{red} of $Fe^{2+/3+}$-ethaline with 0, 5, 10, or 25 wt. % water at 298 K were determined using the inflection point as illustrated in Figure 2a and as listed in Table 1 together with the calculated E_w. In Figure 2b, the peaks at potentials ±0.07 V vs Pt RE in the CV curves represents the cathodic and anodic currents due to the $Fe^{2+/3+}$ redox couple. The E_w of dry $Fe^{2+/3+}$-ethaline is 1.90 V, which is lower than the previously reported value.[35] This discrepancy can be attributed to the difference in the working electrodes used in the experiments. Mu and co-workers employed a glassy carbon working electrode, which tends to yield wider E_w values compared to the platinum working electrode utilized in the current study.[35] The addition of 5 wt. % water in Fe^{2+}/Fe^{3+} -ethaline decreases the electrochemical window by 20 mV. However, addition of 25 wt. % water decreased the electrochemical window by only 30 mV. The small anodic current related to the oxidation of water appears at around -0.9 V vs Pt RE and is likely related to hydrogen oxidation on the reverse scan following water reduction. The cause for the observed decrease in the electrochemical window of $Fe^{2+/3+}$-ethaline upon addition of water is most likely due to the decomposition of H_2O into H_2 and possibly O_2 gas.[36] In dry ethaline, the cathodic decomposition reaction involves electrochemical hydrolysis of ethylene glycol that produces both hydrogen gas and hydroxyl ions.[37,38] As increasing amounts of water are added to $Fe^{2+/3+}$-ethaline, more water tends to decompose to hydrogen and oxygen gases, further narrowing the E_w.

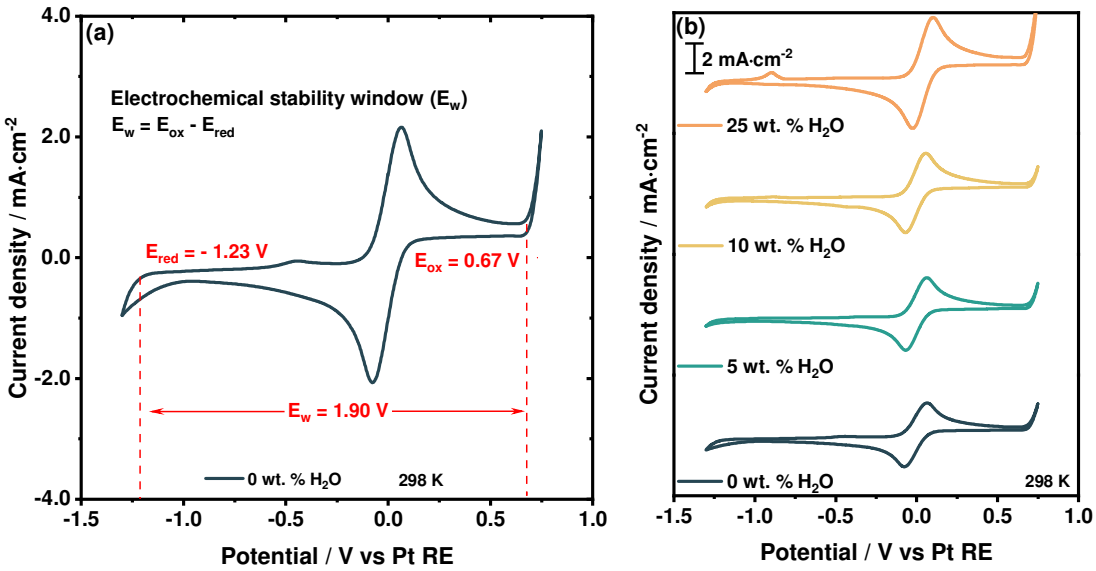

Figure 2. The (a) electrochemical stability windows of the samples were determined by estimating the reduction and oxidation potential limits using the inflection points. (b) CV curves of $Fe^{2+/3+}$-ethaline mixtures containing 0, 5, 10, or 25 wt.% H_2O at a Pt working electrode and at 298 K.

Table 1 shows that the E_w of the $Fe^{2+/3+}$-ethaline mixture is almost maintained even after addition of 25 wt. % water. This suggests that the ethaline/water mixture studied prevents the water molecules to reach the reactive electrode surface, which seems to be dominated by the organic components with the larger electrochemical window. This preferential electrode surface protection prevents the hydrated DES mixture from decomposition and formation of hydrogen and oxygen gases.

Table 1. Cathodic reduction potential limits (E_{red}), anodic oxidation potential limits (E_{ox}), and electrochemical stability windows (E_w) of $Fe^{2+/3+}$-ethaline mixtures containing 0, 5, 10 or 25 wt. % H_2O at 298 K.

Water content (wt. %)	E_{red} (V vs Pt RE)	E_{ox} (V vs Pt RE)	E_w (V)
0	−1.23	0.67	1.90
5	−1.23	0.65	1.88
10	−1.22	0.65	1.87
25	−1.22	0.65	1.87

The ^{1}H NMR and ^{13}C NMR analysis studies in D_2O solvent were carried out for an hour after attempted decomposition at biases of 350 mV beyond anodic and cathodic limiting voltage and found no evidence of degradation of the organic ethaline constituents as observed in Figure S3 and Figure 3, respectively. These findings are different from previous results on DES electrochemical degradation.[37] The absence of detectable cathodic or anodic decomposition products in our NMR analysis is due to the relatively mild potential biads (350 mV). While previous studies used harsher conditions to force decomposition, in this study, we were rather interested in making the system work with minimal to no decomposition. The electrochemical degradation products of the HBD and organic salt would only become detectable under harsher electrolysis conditions. Regardless, it is recommended to pursue further research on the electrochemical stability of DES-water mixtures using a wider range of electrochemical conditions. The ^{1}H NMR and ^{13}C NMR relative peak assignments and the corresponding % H_2O in D_2O at 298 K were summarized in Table S2.

The influence of temperature on the E_w of hydrated $Fe^{2+/3+}$-ethaline mixture was also investigated. As reported in Table S3 and seen in Figure S4, the E_w of the $Fe^{2+/3+}$-ethaline mixture with the same water quantity became marginally narrower as the temperature increased from 298 K to 323 K, which is expected since the redox reaction is thermally activated. The same trend was observed in the case of DES reline (1:2 ChCl:urea) with the addition of 1.0 M $Fe^{2+/3+}$, where the E_w of the mixture became slightly narrower with increasing temperature from room temperature to 323 K. [10]

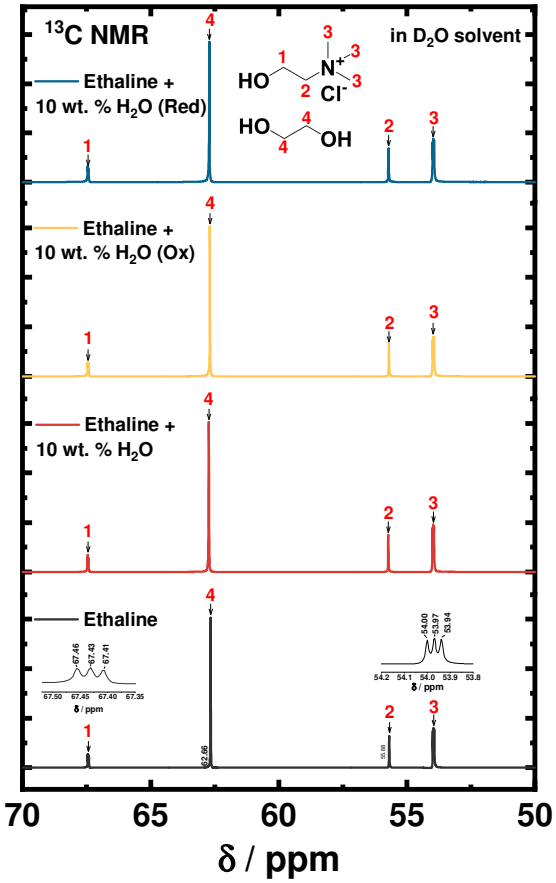

Figure 3. ^{13}C NMR spectra of ethaline, ethaline with 10 wt. % H_2O, oxidized and reduced ethaline with 10 wt. % H_2O in D_2O solvent at 298 K.

3.3. Electron transfer kinetics and mass transport properties

The rotating disk electrode (RDE) is used to measure the kinetic properties of the ethaline solutions containing the $Fe^{2+/3+}$ redox couple at temperature range of 298 K to 323 K. The RDE consists of a disk-shaped electrode that rotates at a controlled speed in the various $Fe^{2+/3+}$-ethaline solutions.[39] By varying the rotation speed of the disk electrode, the kinetics of $Fe^{2+/3+}$ redox reaction can be investigated over a wide range of mass transport conditions. Figure S5-S8 represent the slow-scan linear sweep voltammetry (LSV) measurements of water-containing $Fe^{2+/3+}$-ethaline solutions using Pt RDE at 900 - 2500 rpm rotation speeds. As the rotation speed is increased, the mass transport of the $Fe^{2+/3+}$ redox couple to the electrode surface increases, leading to higher

oxidative and reductive current densities. To estimate the charge transfer coefficients and exchange current density from polarization data, the Tafel equation is conventionally used. However, for fast redox reactions in a highly viscous system, a Tafel analysis would not be able to provide accurate estimates of reaction rate parameters. [40]·[41] Thus, here we applied the extended Butler-Volmer (ex-BV) equation to fit the data (Figure S9-S12) to obtain the kinetic parameters as previously proposed by Shen et al.[41] The LSV measured curve and ex-BV fitting of the driest Fe^{2+}/Fe^{3+}-ethaline mixture at rotation speed of 2200 rpm and temperature of 298 K is shown in Figure 4a. The charge transfer coefficients and exchange current density obtained using this ex-BV method at 298 K to 323 K are listed in Table S4.

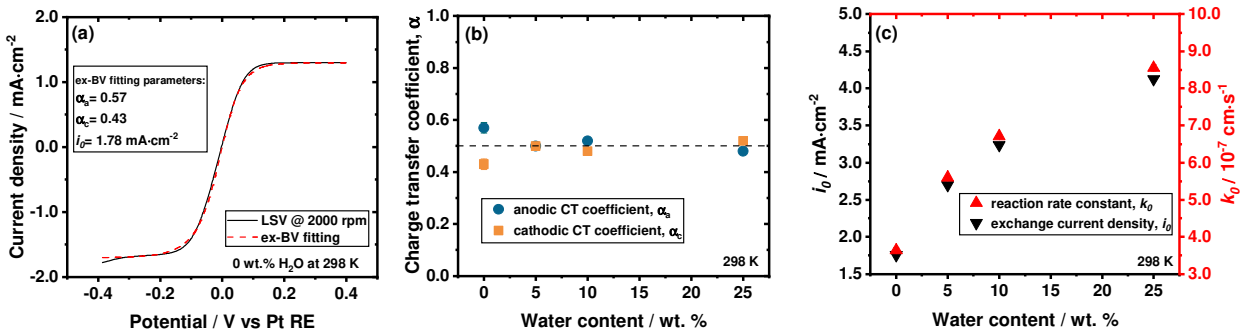

Figure 4. (a) Linear sweep voltammetry curve (solid line) and extended Butler-Volmer fitting (dashed line) of dry Fe^{2+}/Fe^{3+}-ethaline mixture at rotation speed of 2200 rpm at 298 K. The values in the left inset are the anodic charge transfer coefficient (α_a), cathodic charge transfer coefficient (α_c), and exchange current density of the dry sample as determined using the extended Butler-Volmer fitting. (b) α_a, α_c, (c) exchange current density (i_0), and reaction rate constants (k_0) of $Fe^{2+/3+}$-ethaline mixture containing 0, 5, 10, or 25 wt. % H_2O at 298 K.

In Fe^{2+}/Fe^{3+}-ethaline solutions, the anodic (α_a) and cathodic (α_c) charge transfer coefficients describe the efficiency of electron transfer during oxidation ($Fe^{2+} \rightarrow Fe^{3+} + e^-$) and reduction ($Fe^{3+} + e^- \rightarrow Fe^{2+}$) reactions, respectively. Generally, the values of α_a and α_c are between 0 and 1, and a higher value indicates a more efficient electron transfer. It is typically observed that the α_a is larger than α_c in the Fe^{2+}/Fe^{3+} because the anodic oxidation reaction is thermodynamically

favorable and occurs more easily than the cathodic reduction reaction, so the efficiency of electron transfer during the anodic oxidation reaction is usually higher than the cathodic reduction reaction.[42] However, the values of α_a and α_c can depend on various factors such as the electrode material, the electrolyte composition, and the reaction kinetics, so in some specific cases, it is possible for the α_c to be larger than the α_a. In Figure 4b, the α_a is larger than or equal to α_c at water content less than or equal to 10 wt. %, which indicates that the electron transfer during oxidation reaction is more efficient than during the reduction reaction at lower water content. With the addition of 25 wt. % water, the α_a becomes smaller than α_c, which suggests that electron transfer efficiency is reduced during the oxidation reaction compared to the reduction reaction at higher water content. As shown in Figure S13, the charge transfer coefficients are not noticeably impacted by the increase in temperature, as expected for a simple electron transfer reaction.

The exchange current density (i_0) is described as the rate at which Fe^{2+} ions are oxidized to Fe^{3+} ions and Fe^{3+} ions are reduced to Fe^{2+} ions at the same electrode surface. In Figure 4c, the i_0 increases nonlinearly with increasing water, which indicates that addition of water facilitates faster electron transfer between the DES electrolyte and the electrodes. Figure S14 shows the significant impact of the temperature on the i_0 of various Fe^{2+}/Fe^{3+}-ethaline solutions due to the temperature dependence of reaction rate constant, which is related to the activation barrier required for the reaction to occur. Increasing the temperature provides more thermal energy to the system which results in more reactant molecules acquiring enough energy to overcome the activation energy barrier needed for the reaction to occur, leading to an increase in the exchange current density.

The reaction rate constant (k_0) for the Fe^{2+}/Fe^{3+}-ethaline solutions represents the rate at which the forward or reverse reaction between Fe^{2+} and Fe^{3+} ions occurs. Utilizing the i_0 obtained with the extended Butler-Volmer equation,[42] the k_0 can be determined using eq. (4).

$$k_0 = \frac{i_0}{nF[Fe^{3+}]^{1-\alpha_c}[Fe^{2+}]^{\alpha_c}} \quad (4)$$

where n is the number of electrons transferred, F is the Faraday constant (96, 485 A s mol^{-1}), and $[Fe^{3+}]$ and $[Fe^{2+}]$ are the concentrations of Fe^{3+} and Fe^{2+} (mol cm^{-3}) in solution. The k_0 of $Fe^{2+/3+}$ in anhydrous and water-containing ethaline at 298 K are listed in Table S4 and plotted in Figure 4c. The enhancement of k_0 upon introduction of water to the DES mixture is clearly observed in Figure S14 as anticipated due to the direct relationship between i_0 and k_0 as given in eq. (4). With increasing temperature, the k_0 generally also increases because higher temperatures increase the kinetic energy of molecules, which leads to more frequent and energetic collisions between reactant molecules. This increase in the frequency and energy of collisions increases the probability that reactant molecules will react, leading to a faster reaction rate. The observed increase in k_0 of $Fe^{2+/3+}$ -ethaline with increasing temperature has also been reported by Kontturi and colleagues.[43]

The diffusion coefficients play a crucial role in electrochemical processes involving Fe^{2+} and Fe^{3+} ions. The rate of electron transfer reactions at an electrode surface is controlled by the diffusion of the reactant ions, which is influenced by their diffusion coefficients.[44] In Fe^{2+}/Fe^{3+}-ethaline solutions, the diffusion coefficients were determined from limiting current measurements on a Pt RDE at various rotation speeds to examine the kinetics of the reaction and the effect of mass transport on the reaction rate. The ethaline was kept at constant Fe^{3+} and Fe^{2+} concentrations (50 mM), while the water content (0, 5, 10, 25 wt. %) and temperature (298 K – 323 K) were

varied. Using the Levich equation,[42] the diffusion coefficient was calculated from cathodic and anodic limiting currents using eq. (5a) and (5b), respectively.

$$i_{\mathrm{L}}^{c} = -\,0.62\mathrm{nF}D_{\mathrm{Fe^{3+}}}^{2/3}\left(\frac{\eta}{\rho}\right)^{-\frac{1}{6}}\omega^{1/2}[\mathrm{Fe^{3+}}]_{\mathrm{bulk}} \quad (5a)$$

$$i_{\mathrm{L}}^{a} = 0.62\mathrm{nF}D_{\mathrm{Fe^{2+}}}^{2/3}\left(\frac{\eta}{\rho}\right)^{-\frac{1}{6}}\omega^{1/2}[\mathrm{Fe^{2+}}]_{\mathrm{bulk}} \quad (5b)$$

where i_{L} is the limiting current density, n is the number of transferred electrons, F is the Faraday constant, D is the diffusion coefficient, η is the viscosity, ρ is the density, $[\mathrm{Fe}]_{\mathrm{bulk}}$ symbolizes the bulk concentration of $Fe^{2+/3+}$, and ω is the rotation rate expressed as angular velocity.

The computed diffusion coefficients of Fe^{3+} and Fe^{2+} are plotted as a function of water content in Figure 5a and are listed in Table S5 at temperatures between 298 and 323 K. As the water content increases, both the Fe^{3+} and Fe^{2+} ions exhibit an increase in their diffusion coefficients. However, Fe^{2+} ions have a higher diffusion coefficient compared to Fe^{3+} ions at all water contents as seen in Figure S15. At water content ≤ 10 wt. %, the diffusion coefficients for the Fe^{2+} and Fe^{3+} ions in the investigated aqueous ethaline mixtures are still an order of magnitude smaller than their corresponding values in water ($D_{Fe^{2+}}$= 7.19 x 10^{-6} cm^2/s and $D_{Fe^{3+}}$ = 6.04 x 10^{-6} cm^2/s).[25,45]

When DES mixtures are heated, their viscosity decreases, which in turn increases the mobility of the ions and improves their diffusion coefficients. The enhancement in diffusion coefficients with increasing temperature has been supported previously. [43] As temperature increases, the solvent molecules become more disordered and less viscous, which lowers the resistance to the diffusion of ions, reducing the frictional force that impedes their movement and promoting their diffusion through the solvent. The experimental results presented in Figure S16 show that Fe^{2+} diffuses faster than Fe^{3+} in the temperature range of 298 to 303 K.

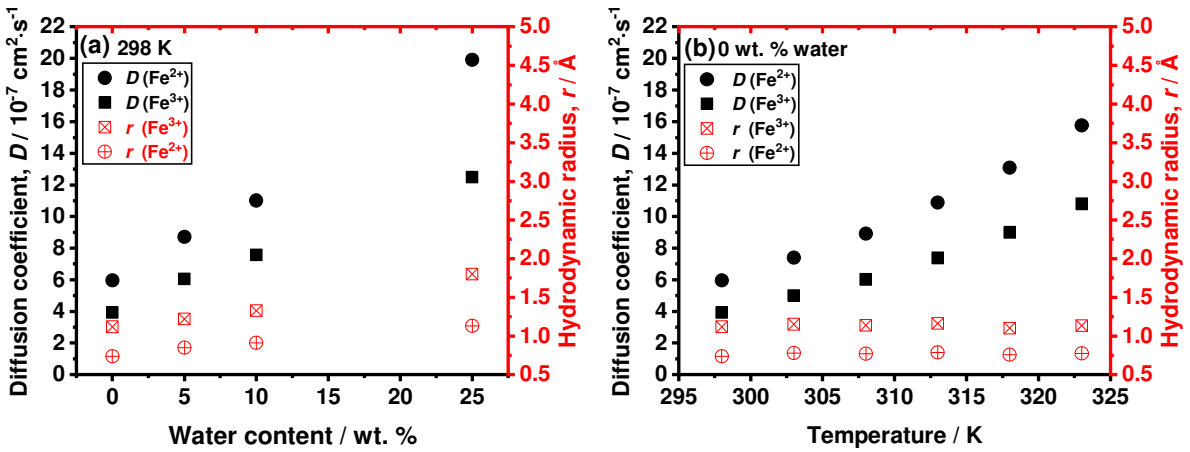

Figure 5. The (a) diffusion coefficients of Fe^{3+} and Fe^{2+} at 298 K, and (b) hydrodynamic radius of Fe^{2+} and Fe^{3+} ions in ethaline containing 0, 5, 10, or 25 wt. % H_2O at 298 – 323 K.

The hydrodynamic radii of Fe^{3+} and Fe^{2+} ions were determined using the Stokes-Einstein equation, which is based on the movement of spherical species in a continuum of solvent restricting the moving ions:[46]

$$r = \frac{k_B T}{6\pi\eta D} \tag{6}$$

Where r is the hydrodynamic radius, k_B is the Boltzmann constant, T is the temperature, η is the temperature-dependent viscosity, and D is the temperature-dependent diffusion coefficient.

The hydrodynamic radii of Fe^{2+} and Fe^{3+} ions at 298 K are calculated to be 0.74 Å and 1.12 Å, respectively. The harder cation Fe^{3+} has the larger hydration shell which is commensurate with its lower diffusion coefficients at all water contents. The hydrodynamic radii of Fe^{3+} and Fe^{2+} ions decrease with increasing temperature as shown in Figure 5b.

3.4. Arrhenius fit and solubility

The temperature dependence of fluidity, conductivity, rate constant, and diffusivity were further investigated using Arrhenius model. The Arrhenius equation assumes linear relationship between log x and inverse of temperature (T^{-1}) as given in eq. (7). [47]

$$\log x = \log A_x - \frac{E_x}{2.303RT} \quad (7)$$

where x refers to various properties such as fluidity (η^{-1}), conductivity (σ), rate constant (k_0), diffusivity of Fe^{2+} ion (D_{Fe2+}) and diffusivity of Fe^{3+} ion (D_{Fe3+}), A_x is the pre-exponential factor, E_x is the activation energy, R is the gas constant, and T is the temperature. Figure S17 depicts the Arrhenius plots for fluidity, conductivity, rate constant, and diffusivity of Fe^{2+} or Fe^{3+} ion at temperature range of 298 – 323 K in 5 K increments. The Arrhenius fit parameters are recorded in Table S6. Figure S18 shows that for water content equal to or less than 10 wt. %, the activation energies for conductivity, rate constant, and diffusivity of Fe^{3+} ion decreases with increasing water content. The activation energy for diffusivity of Fe^{3+} ion exhibits a slightly greater dependence on temperature, followed by conductivity and rate constant. Alternatively, the addition of water does not affect the activation energy for Fe^{2+} diffusivity. At 0 wt. % water, the activation energies for fluidity, conductivity, rate constant, and diffusivity of Fe^{2+} or Fe^{3+} ion are similar, which proposes that the temperature impacts these properties in the same way.

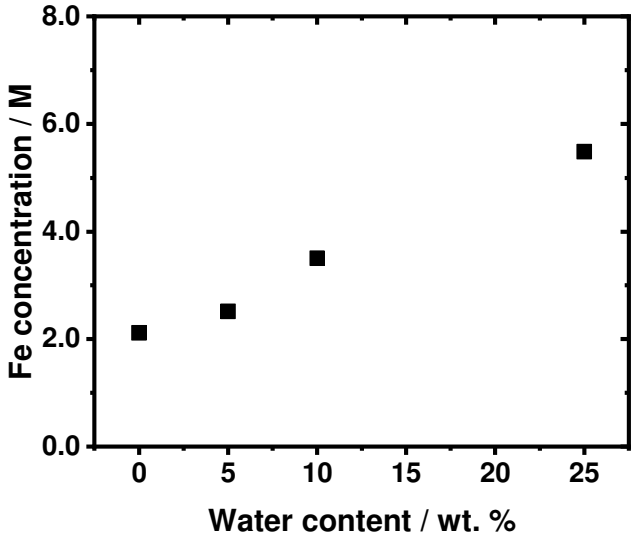

Figure 6. Maximum solubility of $FeCl_2/FeCl_3$ in ethaline as a function of water content.

Furthermore, the solubility of iron chloride salts in ethaline-water mixtures can be observed in Figure 6, which displays the results obtained through atomic absorption spectroscopy. The graph depicts an increase in the solubility of iron chloride salts as the water content in the ethaline solution increases. Because iron chloride salts exhibit high solubility (> 1 M) in DESs, it becomes feasible to utilize the $Fe^{2+/3+}$ redox couple in redox flow batteries.

4. Conclusions

In this work, the electrochemical stability properties of ethaline, a greener electrolyte, were investigated through the redox couple $Fe^{2+/3+}$ as electrochemical probe in light of future use in redox flow batteries. The mass transport parameters ($D_{Fe^{3+}}$, $D_{Fe^{2+}}$) as well as the kinetic parameters such as the charge transfer coefficients (α_a, α_c), exchange current density (i_0), and reaction rate constant (k_0) were determined as a function of gradual addition of water and increase in temperature. The results show that the introduction of defined amounts of water into the DES solvent system at 298 K – 323 K resulted in a decrease in viscosity and density of ethaline, and a three-fold increase in its ionic conductivity. The ~2% decrease in the electrochemical stability window is due to the decomposition of water that produces hydrogen gas. Owing to the lowered viscosity of ethaline, the i_0, k_0, $D_{Fe^{3+}}$ and $D_{Fe^{2+}}$ increased after incorporation of water as minority solvent component into the DES. With an increased temperature, the kinetic energy and mobility of ions were enhanced resulting in an increased i_0, k_0, $D_{Fe^{3+}}$ and $D_{Fe^{2+}}$. The solubility of iron chloride salts in ethaline increases with increasing water content. The activation energy for conductivity, rate constant, and diffusivity of Fe^{3+} ions decrease with water content up to 10 wt. %. However, beyond 10 wt. % water addition, a slight increase in activation energy can be seen. These findings provide an avenue to improve the physical and transport properties of other existing and future DESs by analytical hydration and increasing temperature, without significant reduction in electrochemical stability window, and could lead to the development of an economically viable electrolyte for redox flow batteries. The work presented herein suggests that higher-performance and lower-cost RFBs can be achieved in an environmentally compatible and sustainable manner by a “hydrated-DES” approach.

CRediT authorship contribution statement

Desiree Mae Prado: Conceptualization, Methodology, Validation, Investigation, Formal analysis, Writing – Original Draft. **Xiaochen Shen:** Conceptualization, Methodology, Validation, Investigation, Formal analysis. **Robert Savinell:** Supervision, Conceptualization, Methodology, Writing - Review & Editing. **Clemens Burda:** Supervision, Conceptualization, Methodology, Writing - Review & Editing.

Declaration of competing interest

The authors declare that they have no known competing financial interests or personal relationships that could have appeared to influence the work reported in this paper.

Acknowledgements

DMP would like to thank Prof. Uziel Landau for teaching the electrochemical techniques, Rathiesh Pandian for assisting with the NMR measurements, and Ross Clark Prado for helping with AAS measurements. This work was supported by the Breakthrough Electrolytes for Energy Storage (BEES) – an Energy Frontier Research Center (EFRC) funded by the U.S. Department of Energy, Office of Science, Basic Energy Sciences [grant number DE-SC0019409].

References

[1] B.J. van Ruijven, E. De Cian, I. Sue Wing, Amplification of future energy demand growth due to climate change, Nat. Commun. 10 (2019) 2762. https://doi.org/10.1038/s41467-019-10399-3.

[2] Z. Liu, Z. Deng, S.J. Davis, C. Giron, P. Ciais, Monitoring global carbon emissions in 2021, Nat. Rev. Earth Environ. 3 (2022) 217–219. https://doi.org/10.1038/s43017-022-00285-w.

[3] S. Asiaban, N. Kayedpour, A.E. Samani, D. Bozalakov, J.D.M. De Kooning, G. Crevecoeur, L. Vandevelde, Wind and Solar Intermittency and the Associated Integration Challenges: A Comprehensive Review Including the Status in the Belgian Power System, Energies. 14 (2021) 2630. https://doi.org/10.3390/en14092630.

[4] C. Wu, X.-P. Zhang, M. Sterling, Solar power generation intermittency and aggregation, Sci. Rep. 12 (2022) 1363. https://doi.org/10.1038/s41598-022-05247-2.

[5] B. Dunn, H. Kamath, J. Tarascon, Electrical Energy Storage for the Grid: A Battery of Choices, Science (80-.). 334 (2011) 928–935. https://doi.org/10.1126/science.1212741.

[6] A.F. Zobaa, Energy Storage - Technologies and Applications, InTech, Rijeka, Croatia, 2013. https://doi.org/10.5772/2550.

[7] P. Alotto, M. Guarnieri, F. Moro, Redox flow batteries for the storage of renewable energy: A review, Renew. Sustain. Energy Rev. 29 (2014) 325–335. https://doi.org/10.1016/j.rser.2013.08.001.

[8] A.Z. Weber, M.M. Mench, J.P. Meyers, P.N. Ross, J.T. Gostick, Q. Liu, Redox flow batteries: A review, J. Appl. Electrochem. 41 (2011) 1137–1164. https://doi.org/10.1007/s10800-011-0348-2.
[9] F. Pan, Q. Wang, Redox Species of Redox Flow Batteries: A Review, Molecules. 20 (2015) 20499–20517. https://doi.org/10.3390/molecules201119711.
[10] Q. Xu, L.Y. Qin, Y.N. Ji, P.K. Leung, H.N. Su, F. Qiao, W.W. Yang, A.A. Shah, H.M. Li, A deep eutectic solvent (DES) electrolyte-based vanadium-iron redox flow battery enabling higher specific capacity and improved thermal stability, Electrochim. Acta. 293 (2019) 426–431. https://doi.org/10.1016/j.electacta.2018.10.063.
[11] M.H. Chakrabarti, F.S. Mjalli, I.M. Alnashef, M.A. Hashim, M.A. Hussain, L. Bahadori, C.T.J. Low, Prospects of applying ionic liquids and deep eutectic solvents for renewable energy storage by means of redox flow batteries, Renew. Sustain. Energy Rev. 30 (2014) 254–270. https://doi.org/10.1016/j.rser.2013.10.004.
[12] L. Bahadori, M.A. Hashim, N.S.A. Manan, F.S. Mjalli, I.M. AlNashef, N.P. Brandon, M.H. Chakrabarti, Investigation of Ammonium- and Phosphonium-Based Deep Eutectic Solvents as Electrolytes for a Non-Aqueous All-Vanadium Redox Cell, J. Electrochem. Soc. 163 (2016) A632–A638. https://doi.org/10.1149/2.0261605jes.
[13] B.B. Hansen, S. Spittle, B. Chen, D. Poe, Y. Zhang, J.M. Klein, A. Horton, L. Adhikari, T. Zelovich, B.W. Doherty, B. Gurkan, E.J. Maginn, A. Ragauskas, M. Dadmun, T.A. Zawodzinski, G.A. Baker, M.E. Tuckerman, R.F. Savinell, J.R. Sangoro, Deep Eutectic Solvents: A Review of Fundamentals and Applications, Chem. Rev. 121 (2021) 1232–1285. https://doi.org/10.1021/acs.chemrev.0c00385.
[14] E.L. Smith, A.P. Abbott, K.S. Ryder, Deep Eutectic Solvents (DESs) and Their Applications, Chem. Rev. 114 (2014) 11060–11082. https://doi.org/10.1021/cr300162p.
[15] B.E. Gurkan, E.J. Maginn, E.B. Pentzer, Deep eutectic solvents: A new class of versatile liquids, J. Phys. Chem. B. 124 (2020) 11313–11315. https://doi.org/10.1021/acs.jpcb.0c10099.
[16] H. Musarurwa, N.T. Tavengwa, Deep eutectic solvent-based dispersive liquid-liquid micro-extraction of pesticides in food samples, Food Chem. 342 (2021) 127943. https://doi.org/10.1016/j.foodchem.2020.127943.
[17] J. Płotka-Wasylka, M. de la Guardia, V. Andruch, M. Vilková, Deep eutectic solvents vs ionic liquids: Similarities and differences, Microchem. J. 159 (2020) 105539. https://doi.org/10.1016/j.microc.2020.105539.
[18] M.A. Miller, J.S. Wainright, R.F. Savinell, Iron Electrodeposition in a Deep Eutectic Solvent for Flow Batteries, J. Electrochem. Soc. 164 (2017) A796–A803. https://doi.org/10.1149/2.1141704jes.
[19] G. Cui, D. Yang, H. Qi, Efficient SO2Absorption by Anion-Functionalized Deep Eutectic Solvents, Ind. Eng. Chem. Res. 60 (2021) 4536–4541. https://doi.org/10.1021/acs.iecr.0c04981.
[20] H. Ren, C. Chen, S. Guo, D. Zhao, Q. Wang, Synthesis of a Novel Allyl-Functionalized Deep Eutectic Solvent to Promote Dissolution of Cellulose, BioResources. 11 (2016) 8535–8547. https://doi.org/10.15376/biores.11.4.8457-8469.
[21] L. Li, K. Liu, H. Xing, X. Li, Q. Zhang, D. Han, H. He, H. Yan, B. Tang, Deep eutectic solvents functionalized polymers for easily and efficiently promoting biocatalysis, J. Catal. 374 (2019) 306–319. https://doi.org/10.1016/j.jcat.2019.05.006.
[22] Y. Liu, Q. Zhang, G.O. Odunmbaku, Y. He, Y. Zheng, S. Chen, Y. Zhou, J. Li, M. Li, K.

Sun, Solvent effect on the Seebeck coefficient of Fe^{2+}/Fe^{3+} hydrogel thermogalvanic cells, J. Mater. Chem. A. (2022) 19690–19698. https://doi.org/10.1039/d1ta10508f.
[23] L. Li, A. Ghahreman, The Synergistic Effect of Cu^{2+}-Fe^{2+}-Fe^{3+} Acidic System on the Oxidation Kinetics of Ag-Doped Pyrite, J. Phys. Chem. C. 122 (2018) 26897–26909. https://doi.org/10.1021/acs.jpcc.8b06727.
[24] D. Inoue, T. Komatsu, H. Niwa, T. Ina, H. Nitani, H. Abe, Y. Moritomo, Coordination States of Fe^{3+} and Fe^{2+} Dissolved in Organic Solvents , J. Phys. Soc. Japan. 91 (2022). https://doi.org/10.7566/jpsj.91.094605.
[25] M. Spiro, A.M. Creeth, Tracer Diffusion Coefficients of I^-, I_3^-, Fe^{2+} and Fe^{3+} at Low Temperatures, J. Chem. Soc. Faraday Trans. 86 (1990) 3573–3576.
[26] R. Demir-Cakan, M.R. Palacin, L. Croguennec, Rechargeable aqueous electrolyte batteries: from univalent to multivalent cation chemistry, J. Mater. Chem. A. 7 (2019) 20519–20539. https://doi.org/10.1039/C9TA04735B.
[27] G.J. Chung, J. Han, S.-W. Song, Fire-Preventing $LiPF_6$ and Ethylene Carbonate-Based Organic Liquid Electrolyte System for Safer and Outperforming Lithium-Ion Batteries, ACS Appl. Mater. Interfaces. 12 (2020) 42868–42879. https://doi.org/10.1021/acsami.0c12702.
[28] M.C. Figueiredo, Towards the sustainable synthesis of ethylene glycol, Nat. Catal. 3 (2020) 4–5. https://doi.org/10.1038/s41929-019-0418-0.
[29] J. Zhang, J. Huang, L.A. Robertson, R.S. Assary, I.A. Shkrob, L. Zhang, Elucidating Factors Controlling Long-Term Stability of Radical Anions for Negative Charge Storage in Nonaqueous Redox Flow Batteries, J. Phys. Chem. C. 122 (2018) 8116–8127. https://doi.org/10.1021/acs.jpcc.8b01434.
[30] I. Alfurayj, C.C. Fraenza, Y. Zhang, R. Pandian, S. Spittle, B. Hansen, W. Dean, B. Gurkan, R. Savinell, S. Greenbaum, E. Maginn, J. Sangoro, C. Burda, Solvation Dynamics of Wet Ethaline: Water is the Magic Component, J. Phys. Chem. B. 125 (2021) 8888–8901. https://doi.org/10.1021/acs.jpcb.1c04629.
[31] R. Cheng, P. Sun, H. Su, W. Yang, P. Leung, Q. Xu, Effect of exerted magnetic field on the performance of non-aqueous iron-vanadium redox flow battery with deep eutectic solvent (DES) electrolyte, Electrochim. Acta. 399 (2021) 139404. https://doi.org/10.1016/j.electacta.2021.139404.
[32] C. Schreiner, S. Zugmann, R. Hartl, H.J. Gores, Fractional walden rule for ionic liquids: Examples from recent measurements and a critique of the so-called ideal KCl line for the walden plot, J. Chem. Eng. Data. 55 (2010) 1784–1788. https://doi.org/10.1021/je900878j.
[33] P. Sun, P. Lu, J. Xu, Q. Ma, W. Zhang, A.A. Shah, H. Su, W. Yang, Q. Xu, The influence and control of ultrasonic on the transport and electrochemical properties of redox couple ions in deep eutectic solvent (DES) for redox flow battery application, Electrochim. Acta. 394 (2021) 139140. https://doi.org/10.1016/j.electacta.2021.139140.
[34] J.M. Klein, H. Squire, W. Dean, B.E. Gurkan, From Salt in Solution to Solely Ions: Solvation of Methyl Viologen in Deep Eutectic Solvents and Ionic Liquids, J. Phys. Chem. B. 124 (2020) 6348–6357. https://doi.org/10.1021/acs.jpcb.0c03296.
[35] Q. Li, J. Jiang, G. Li, W. Zhao, X. Zhao, T. Mu, The electrochemical stability of ionic liquids and deep eutectic solvents, Sci. China Chem. 59 (2016) 571–577. https://doi.org/10.1007/s11426-016-5566-3.
[36] B.H. Robb, S.E. Waters, M.P. Marshak, Evaluating aqueous flow battery electrolytes: a coordinated approach, Dalt. Trans. 49 (2020) 16047–16053.

https://doi.org/10.1039/d0dt02462g.
[37] N.S. Sinclair, X. Shen, E. Guarr, R.F. Savinell, J.S. Wainright, Electrochemical Decomposition of Primary Alcohol Groups in Deep Eutectic Solvents, J. Electrochem. Soc. 168 (2021) 106506. https://doi.org/10.1149/1945-7111/ac2d14.
[38] K. Haerens, E. Matthijs, K. Binnemans, B. Van der Bruggen, Electrochemical decomposition of choline chloride based ionic liquid analogues, Green Chem. 11 (2009) 1357–1365. https://doi.org/10.1039/b906318h.
[39] J.L. Town, F. MacLaren, H.D. Dewald, Rotating disk voltammetry experiment, J. Chem. Educ. 68 (1991) 352–354. https://doi.org/10.1021/ed068p352.
[40] N.A. Shaheen, M. Ijjada, M.B. Vukmirovic, R. Akolkar, Mechanism of Electrochemical Oxidation of Nitroxide Radicals in Ethaline Deep Eutectic Solvent, J. Electrochem. Soc. 167 (2020) 143505. https://doi.org/10.1149/1945-7111/abc439.
[41] X. Shen, N. Sinclair, J. Wainright, R.F. Savinell, Methods—Analyzing Electrochemical Kinetic Parameters in Deep Eutectic Solvents Using an Extended Butler-Volmer Equation, J. Electrochem. Soc. 168 (2021) 056520. https://doi.org/10.1149/1945-7111/ac006a.
[42] A.J. Bard, L.R. Faulkner, Electrochemical Methods: Fundamentals and Applications, 2nd ed., John Wiley & Sons, Inc, Hoboken, NJ, 2001. ISBN 0471043729
[43] D. Lloyd, T. Vainikka, M. Ronkainen, K. Kontturi, Characterisation and application of the Fe(II)/Fe(III) redox reaction in an ionic liquid analogue, Electrochim. Acta. 109 (2013) 843–851. https://doi.org/10.1016/j.electacta.2013.08.013.
[44] Q. Ma, C. Mao, L. Zhao, Z. Chen, H. Su, Q. Xu, A pore-scale study for reactive transport processes in double-layer gradient electrode as negative side of a deep eutectic solvent electrolyte-based vanadium-iron redox flow battery, Electrochim. Acta. 431 (2022) 141110. https://doi.org/10.1016/j.electacta.2022.141110.
[45] M.A. Ribeiro, A.C.F, Sobral, A.J.F.N., Santos, C.I.A.V., Lobo, V. M.M, Cabral, A.M.T.D.P.V., Veigam F.J.B., Esteso, Calculations of Diffusion Coefficients of Iron Salts in Aqueous Solutions at 298. 15 K : A Useful Tool for the Knowledge of the Structure of these Systems, Acta Ch. 59 (2012) 353–358.
[46] A. Das, S.M. Ali, Unusual behavior of Stokes-Einstein relation in liquid mixtures, AIP Adv. 10 (2020). https://doi.org/10.1063/5.0004572.
[47] K.J. Laidler, The development of the arrhenius equation, J. Chem. Educ. 61 (1984) 494–498. https://doi.org/10.1021/ed061p494.